Catalysis Today 148 (2009) 55–62

Contents lists available at ScienceDirect

Catalysis Today

journal homepage: www.elsevier.com/locate/cattod

Synthesis of hybrid (Ni-Mo)carbides/carbon-coated mesoporous materials and their catalytic properties for hydrocracking of intermediate paraffins (n-C_8)

A.I. Reyes de la Torre [a], J.M. Domínguez [a], J.A. Melo-Banda [b,*], C.E. Ramos G. [b], G. Sandoval [b], R.C. Ángeles [a], M. Torres Rodriguez [c]

[a] Instituto Mexicano del Petróleo, Programa de Ingeniería Molecular, 152 Eje Central L. Cárdenas, C.P. 07730 México D.F., Mexico
[b] Instituto Tecnológico de Ciudad Madero, Juventino Rosas y Jesús Urueta S/N Col. Los Mangos, C.P. 89440 Cd. Madero, Mexico
[c] Universidad Autónoma Metropolitana de Azcapotzalco, San Pablo 180, Col. Reynosa Tamaulipas, Del. Azcapotzalco, C.P. 02200 México D.F., Mexico

ARTICLE INFO

Article history:
Available online 15 August 2009

Keywords:
Polyacrylonitrile
Carbonization
NiMo
Carbide
n-Paraffin
Hydrocracking

ABSTRACT

This work explores the structure and physical chemistry of hybrid materials formed by casting of carbon precursors (*i.e.*, acrylonitrile, AN) in mesoporous MCM-41 type siliceous materials. After polymerization and carbonization hollow carbonaceous fibers were formed and these were impregnated with Ni and Mo salts, *i.e.*, 2.8 atoms Mo/nm^2 and Ni/(Ni + Mo) ratio equal to 0.5. The supported metal carbides were characterized by XRD, BET, NH_3-TPD and HRTEM and evaluated for the catalytic hydrocracking of intermediate straight chain model paraffins (i.e. n-octane) at 673 K, P = 1 atm. The overall activity and selectivity of the NiMoC/PAN-P catalysts for n-C_8 hydrocracking were distinct with respect to other catalysts of reference, *i.e.*, NiMo/Al_2O_3. In particular, carbon nanofibers and lower hydrocarbons (*i.e.*, from propane to n-heptane) are the products formed by the successive dehydrogenation, cracking and carbon atoms diffusion through the metal particles.

1. Introduction

The increasing abundance of reduced heavy crude oil poses serious challenges for the transport and processing of these fractions. For example, the typical Maya crude oil has a density of about 22°API, a sulfur content above 3 wt.%, a content of metals of about 400 ppm (V + Ni) and a Ramsbottom carbon number of around 16. These properties cause serious difficulties for handling and processing the oil fractions by means of conventional refining processes [1]. For this, more severe conditions are usually applied for upgrading the physical and chemical properties of reduced crude oil fractions while complying environmental legislation. Usually, the modification of the plant design and use of new catalysts with higher capacity for withstanding the severe operating conditions are being applied in the reduced crude oils refining and further investigations on the factors influencing the catalysts performance are being carried out [1]. In this context, the trend in hydrotreating heavy crude oil is to improve the quality of the crude while hydrocracking is the process of choice for upgrading heavy oil fractions and barrel bottom residues by promoting hydrogenation and cracking of long-chain molecules [2]. Supported metal sulfides from groups VI and VIII have been widely studied for their abilities to promote hydrogenation, however, the complex bulky molecules that are typical of petroleum residues and heavy cuts are polynuclear aromatics, naphtenes and asphaltenes, some of which tend to be refractory under conventional processing conditions. Furthermore, the fluid transport and dynamics of these complex molecules impose diffusion constraints that limit the yield of catalytic reactions, thus, the design of new catalysts must look at supports with a wide open porous system in order to give access to the bulky molecules while keeping a high thermal stability and supported metal active phases that withstand the severe reaction conditions without sintering or combining chemically with the support phase [3–5]. In this context the present study explores the synthesis and properties of new ceramic-like phases composed by Ni-Mo carbides supported on mesoporous carbon fibers, which were synthesized by the casting of acrylonitrile (AN) precursors on diverse siliceous matrixes, *i.e.*, MCM-41, SBA15, IMP-1, and IMP-2 type materials [6–9]. These materials were tested for the catalytic hydrocracking of long-chain linear paraffin using n-C_8 as a molecular model and a fixed bed reactor system at atmospheric pressure.

Also, the structural and textural properties of these novel mesoporous refractory systems, which are composed by the carbonaceous supports and the metal active phases were characterized by several techniques, including XRD, High Resolution Transmission Electron Microscopy (HRTEM) and N_2-adsorption (BET).

* Corresponding author. Tel.: +52 833 2215020; fax: +52 833 215 8544.
E-mail address: melobanda@yahoo.com.mx (J.A. Melo-Banda).

0920-5861/$ – see front matter. Crown Copyright © 2009 Published by Elsevier B.V. All rights reserved.
doi:10.1016/j.cattod.2009.05.006

2. Experimental

Siliceous mesoporous materials with hexagonal and cubic pore arrays (*i.e.*, MCM-41 and MCM-48) and novel materials with a radial pore distribution (*i.e.*, IMP-1 and IMP-2) were prepared at room temperature according to previous reports by Terrés and co-workers [9] and Volpe et al. [10]. All the materials reported on this work were synthesized in our laboratories, some of them, *i.e.*, IMP-1 and IMP-2, were reported for the first time by our group [9a,9b]. These mesoporous materials were intercalated with AN, which was polymerized "in-situ" using benzoyl peroxide as the initiator (12/1 molar ratio) under a N_2 environment at room temperature. Then, these materials were carbonized under N_2 at 1273 K and were labeled with "P" at the end, *i.e.*, from "pyrolized" or "carbonized". For example "MCM-41-PAN-P" means a siliceous MCM-41 type material that was impregnated with AN and then was polymerized and carbonized subsequently (P). These composite materials were used as supports of Ni and Mo metals that were impregnated from inorganic salts solutions, *i.e.*, $(NH_4)_6Mo_7O_{24}{\cdot}4H_2O$ (Aldrich Chemical Co., 99.97%) and $(NO_3)_2.6H_2O$ (Aldrich Chemical Co., 99.97%), afterward the materials were calcined at 773 K. In this case the labels were as (NiMo)C/MCM-41-PAN-P, which means a supported metal (Ni,Mo) catalyst on the support MCM-41-PAN-P. Also, some supports are labeled as "F" or "S", for example MCM-41-PAN-P (F) refers to catalysts that were submitted to a "flash treatment" or a very rapid introduction of the solid into an oven heated at 1273 K for a minute, while the label MCM-41-PAN-P (S) refers to catalysts submitted to a "slow carbonization" treatment at 1273 K. For all the cases ammonium phosphate in a proportion of about 2% was used as a doping agent, which was incorporated by the incipient wetness technique. These materials were treated with reducing agents like anhydrous ammonia (NH_3, 99.99% purity) and a combination of 1 part of hydrogen (H_2) diluted in 2 parts of methane (CH_4), *i.e.*, $CH_4/H_2 = 2/1$, which is a reduction procedure reported elsewhere [10]. After reduction all the solids loaded with metals were passivated under a diluted flow of oxygen (O_2: 1 vol.%) combined with argon (Ar) in order to avoid spontaneous combustion in air. All these catalysts were prepared with a total metal content of 2.8 metal atoms/nm^2, where the surface area of each initial support, before polymerization and carbonization treatments, was used to calculate the metals content according to a specific atomic ratio, *i.e.*, Ni/(Ni + Mo) = 0.5 [11]. The powder X-Ray Diffraction (XRD) patterns were obtained using a Bruker (Axs) diffractometer (Model D8 ADVANCE). Other physical and chemical properties of these materials were characterized by XRD using a diffractometer Siemmens D-500 (λ_{CuK} = 1.54 Å), while the textural properties were determined by N_2 adsorption (BET and BJH methods), at 77 K, by means of a Micromeritics Instrument ASAP-2000. Fenelonov's method [11] was used for determining the wall thickness of the mesoporous materials and FTIR was applied for determining the surface acidity of the supported catalysts using a Nicolet Avantar diffuse reflectance spectrometer. Scanning and Transmission Electron Microscopy techniques were performed using a Philips XL30ESEM and JEM-2200FS Jeol for the structural and compositional characterization of the solids. Programmed thermal desorption of ammonia (NH_3-TPD) was used for determining the surface acidity strength of the catalysts, using an apparatus from In-Situ-Research Instruments (ISRI), Model Rig-100-19, which is used for determining the amount of ammonia (NH_3) desorbed in function of temperature, in the interval starting from room temperature to 600 °C. A series of peaks with distinct height (*i.e.* arbitrary units) and width (ΔT) indicate the appearance of desorbed ammonia, which depends on the adsorption strength for each sample. Also, the hydrothermal stability was tested under air stream with 100% relative humidity at 873 K for 3 h [10]. The catalysts performance was determined using a fixed-bed reactor system fitted with an Agilent HP 6890 GC and the conversion of n-octane at 673 K and P = 1 atm was followed for each catalyst. In all these cases the amount of catalysts in the reactor was 0.3 g, which were activated at 723 K under hydrogen stream (1.8 L h^{-1}) before carrying out the reaction, while the hydrogen flow during the reaction was controlled for obtaining a contact time of 3282 s^{-1}. The evaluation conditions included a reaction temperature of 673 K, a temperature of the reactant saturator of 310 K and activation at 723 K for 3 h under hydrogen flow and a preliminary reaction period of 50 h.

3. Results

3.1. General structural properties

Fig. 1 illustrates the X-ray diffraction pattern of the parent support MCM-41 with a typical periodicity $d \sim 35.8$ Å, which arises from the pores array. In comparison, Fig. 2 illustrates the X-ray diffraction features corresponding to the series of supports treated for polymerization and carbonization of the precursor (AN) supported on the siliceous materials, *i.e.*, MCM-41-PAN-P (723 K), MCM-41-PAN-P (1023 K), MCM-41-PAN-P (F) (*i.e.*, "F" means "flash-treated") at 1273 K and MCM-41-PAN-P (S) (*i.e.*, "S" means "slow carbonization" at 1273 K). All the XRD patterns in Fig. 2 show similar features with respect to the initial MCM-41 type porous structure, as illustrated in Fig. 1, even for those materials that were treated at extreme conditions, *i.e.*, carbonization at 1023–1273 K. In addition, Fig. 3 shows the XRD patterns of the metal catalysts based upon (NiMo)C/MCM-41-PAN-P (metal ratios of 0.5, with and without phosphorous: 2% P) and one observes a partial segregation of the Ni and Mo carbide phases, as well as the presence of some traces of $NiMoO_4$, which was verified by the J. C. P. D. S. File 18-0879 [10,12]. In Fig. 3, the XRD peaks appearing at 44.5° and 51.9°(2θ) correspond to the NiC phase which has a cubic symmetry (J.C.P.D.S. File 14-0020). In addition, the peaks appearing within the interval $53.5° \leq 2\theta \leq 75.3°$ correspond to the MoC phase, which has a hexagonal symmetry (J.C.P.D.S. 08-0384). In summary, the XRD results displayed in Figs. 1–3 lead us to conclude that the severe oxidative treatment at 723–1023 K and the additional treatment at 1273 K for 2 h do not modify extensively the pore arrays but the main periodicity withstands at $d \approx 35.8$ Å, similar to the initial MCM-41 materials. Also, the

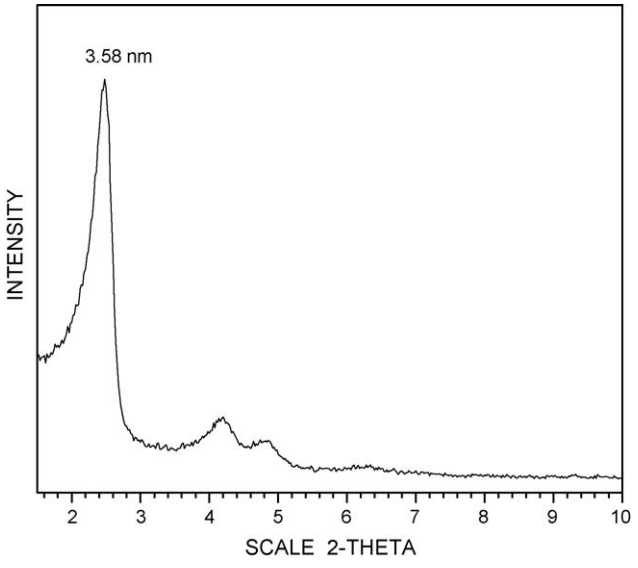

Fig. 1. X-ray diffraction pattern of the initial support MCM-41.

Table 1
Structural and textural properties of the initial MCM-41 type support and the MCM-41 materials loaded with AN, polymerized and carbonized at various temperatures.

Sample	d_{100} (Å)	a_0 (Å)	S_t ($m^2 g^{-1}$)	S_{ext} ($m^2 g^{-1}$)	S_{me} ($m^2 g^{-1}$)	V_{me} ($cm^3 g^{-1}$)	D_{me} (Å)	H_w (Å)	D_p (Å)	V_t ($cm^3 g^{-1}$)
MCM-41	36	41.3	923	40	883	0.7	34	7.2	35	0.8
MCM-41-PAN-P-723	36	41.3	899	51	848	0.6	29	12.2	30	0.7
MCM-41-PAN-P-1023	36	41.6	533	64	469	0.3	30	11.1	45	0.6
MCM-41-PAN-P 1273-F	35	40.6	513	57	456	0.3	29	11.1	44	0.6
MCM-41-PAN-P-1273-S	37	41.1	393	12	382	0.2	23	18.4	29	0.3

a_0 = unit (hexagonal) cell. d_{100} = interplanar distance. S_{me} = area of mesopores. V_{me} = volume of mesopores. D_{me} = diameter of mesopores by Felenov's method. H_w = pore wall thickness.

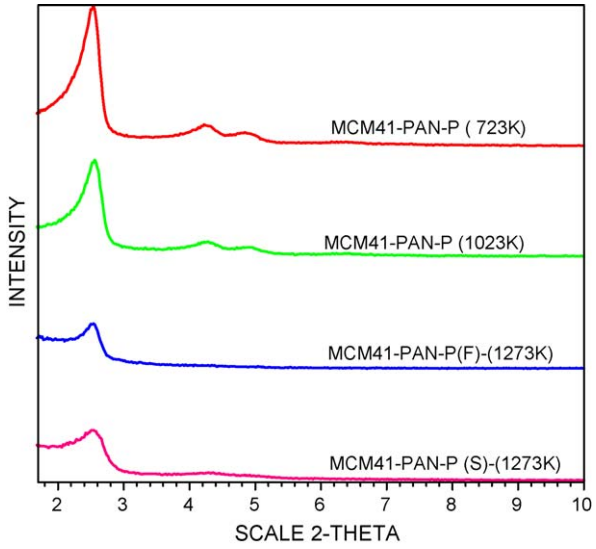

Fig. 2. X-ray diffraction patterns of the support (carbonized) MCM-41-PAN-P (723 K), MCM-41-PAN-P (1023 K), MCM-41-PAN-P (s) flash-treated at 1273 K and MCM-41-PAN-P (L) treated at 1273 K (slow carbonization).

subsequent treatments of the supported metal catalysts lead to the formation of NiC and MoC (*i.e.*, metal carbides) which are segregated form each other.

3.2. Textural properties

Table 1 illustrates the main textural properties of the initial supports together with the materials loaded with acrylonitrile, polymerized and carbonized. As observed, the post-synthesis treatments cause a drastic decrease of the surface area of these materials with respect to the initial MCM-41 matrix, thus leaving

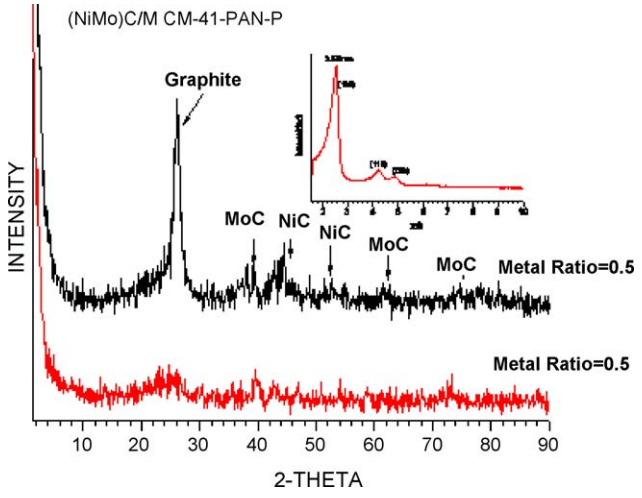

Fig. 3. X-ray diffraction patterns of (NiMo)C/MCM-41-PAN-P (carbonized).

Table 2
Textural properties of supports and catalysts after carbonization and incorporation of metals (Ni,Mo) respectively.

Supports and catalysts	Surface Area ($m^2 g^{-1}$)	Pore volume ($cm^3 \cdot g^{-1}$)	Pore diameter (Å)
MCM-41	923	0.8	35
MCM-41-PAN-P	899	0.7	30
NiMoC/MCM-41-PAN-P Rel.0.5, 2% P	180	0.2	48
NiMoC/MCM-48-PAN-P Rel.0.3, 2% P	162	0.2	57
NiMoC/IMP-1-PAN-P Rel.0.5, 2% P	215	0.3	63
NiMoC/IMP-2-PAN-P Rel.0.5, 2% P	110	0.3	98
NiMoC/SBA-15-PAN-P Rel.0.5, 2% P	128	0.3	83

about one-third of the original area. Similarly, the supported metal carbides follow this trend (Table 2), for example, the surface area of (Ni-Mo)C/MCM-41-PAN-P (metal ratio of 0.5, with 2 wt% P) is only 19% of the surface area of the initial material and 45% of the surface area of the carbonized support (MCM-41-PAN-P). Also, Table 2 illustrates the textural properties of the metal catalysts containing the NiMo series supported on the carbonized supports MCM-41-PAN-P, MCM-48-PAN-P, IMP-1-PAN-P, IMP-2-PAN-P, and SBA-15-PAN-P. In contrast, the total pore volume of the (Ni-Mo)C/MCM-41-PAN-P materials was reduced for bout 33% with respect to the carbonized support MCM-41-PAN-P and about 75% respect to the initial MCM-41 support, while the mean pore diameters of the supported metal carbides increase from 28% up to about three times of the original diameters of the initial MCM-41 supports, which might be a consequence of partial pore coalescence. During the carbonization process the decrease of pore volume of the series MCM-41-PAN-P may be due to partial blockage of pores. Also, Fig. 4 shows that carbonization of PAN causes a negative variation of the number of pores in the interval around 27 Å (diameter), which could indicate the total blockage of those pores. In addition, the wall thickness (H_w) corresponding to the initial MCM-41 and the

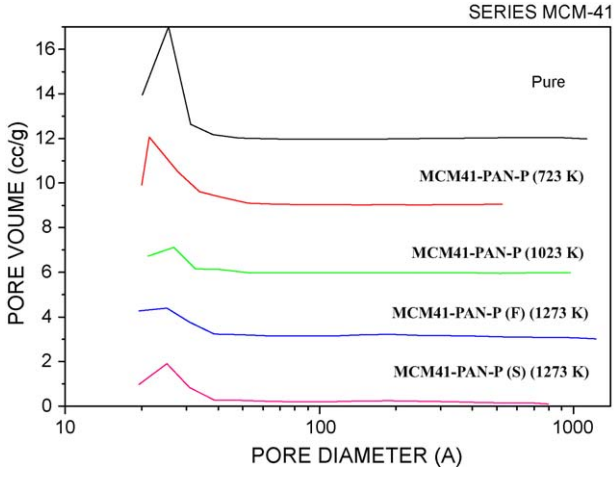

Fig. 4. Pore diameters distribution of initial MCM-41 and carbonized MCM-41-PAN-P at different temperatures.

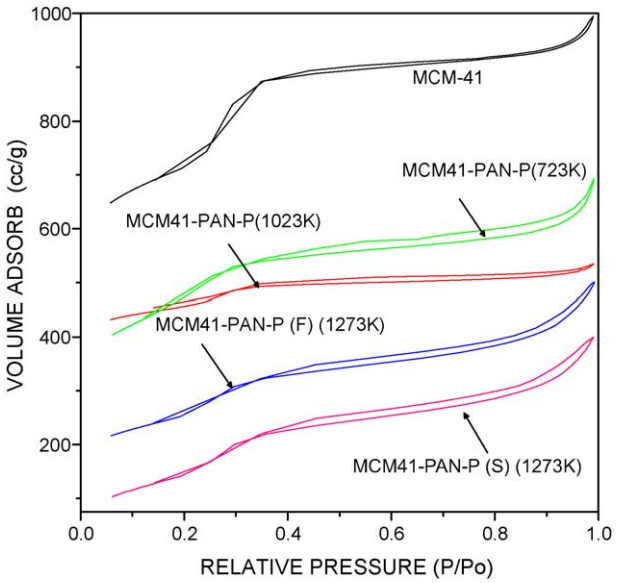

Fig. 5. Adsorption–desorption isotherms of initial MCM-41 and MCM-41-PAN-P (carbonized) at different temperatures.

carbonized MCM-41 (PAN-P) supports was determined by Fenelonov's method (Table 2) and, as observed, the MCM-41(PAN-P) materials have a wall thickness of 18.4 Å, that is about 2.5 times thicker than initial MCM-41. The lower surface area and pore volume of the carbonized materials may be explained by carbon deposition on the pores mouth and formation of a carbonaceous layer into the pore system (see Tables 1 and 2). Also, Fig. 5 illustrates the adsorption isotherms of MCM-41 and MCM-41(PAN-P), which are type IV isotherms with a typical Langmuir type profile, as reported elsewhere for the former MCM-41 type material [6,7], but one observes that the adsorption isotherm of the (NiMo)C/MCM-41-PAN-P catalyst shows a different profile with respect to the precursor mesoporous materials (MCM-41). For example, the classical step at about P/Po = 0.3 is milder in the case of the carbonized materials, thus indicating a smoother transition between distinct pore sizes and less defined pore size distribution with respect to the MCM-41 type materials.

3.3. Acid properties

Table 3 shows the total acidity expressed in μmol NH_3/g and μmol NH_3/m^2 for the supported NiMo bimetallic carbide catalysts and various mesoporous materials (MCM-41, MCM-48, IMP-1, IMP-2, SBA-15). The acidity ranges from 35 to 130 μmol NH_3/g. Also, Table 4 and Fig. 6 show the distribution of the acid sites for the NiMo bimetallic carbides supported on MCM-41-PAN-P. In turn, the NiMoC/MCM-41-PAN (metal ratio of 0.5, with 2% P) and NiMoC/MCM-48-PAN (Metal ratio of 0.5, with 2% P) catalysts show NH_3 desorption curves with the outstanding behavior of the latter

Table 3
Total surface acidity determined by NH_3-TPD for the metal supported catalysts series.

Catalysts (metal ratio = 0.5, 2% P)	Acidity	
	(μmol NH_3 g^{-1})	(μmol NH_3 m^{-2})
NiMoC/MCM-48-PAN-P	130	0.72
NiMoC/MCM-41-PAN-P	77	0.42
NiMoC/IMP-1-PAN-P	65	0.59
NiMoC/IMP-2-PAN-P	35	0.16
NiMoC/SBA-15-PAN-P	117	0.92

Table 4
Distribution of acidity strength for the metal catalysts supported on the carbonized supports.

Catalyst (metal ratio = 0.5, 2% P)	Strong (%)	Medium (%)	Weak (%)
NiMoC/MCM-41-PAN-P	21	22	57
NiMoC/MCM-48-PAN-P	12	36	52
NiMoC/IMP-1-PAN-P	19	26	55
NiMoC/IMP-2-PAN-P	17	27	56
NiMoC/SBA-15-PAN-P	13	28	59

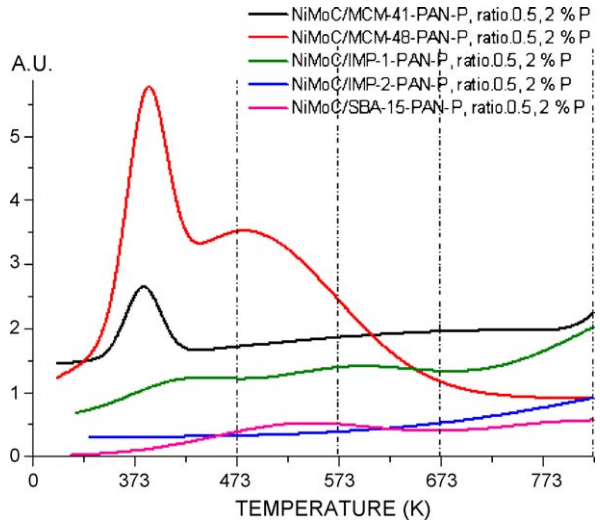

Fig. 6. Thermal Programmed Desorption (TPD) curves of NiMo bimetallic catalyst supported on carbonized MCM-41, MCM-48, IMP-1, IMP-2 and SBA-15 materials.

material, while the rest of the solids show a similar behavior. The presence of those acidic sites is a consequence of the combination of the metal with the phosphorous content as well as the presence of hollow carbon fibers [12,13].

The IR spectra of the mesoporous supports (MCM-41, MCM-48-IMP-1, IMP-2, and SBA-15) indicate that the high carbonization temperatures cause a diminution of the band intensity in the region of the OH groups at 3380 cm^{-1} and the functional groups of PAN disappear, as shown by Fig. 7.

It is probable that a part of the acid (or basic) sites are located on the functional groups of the carbon surface as a consequence of the

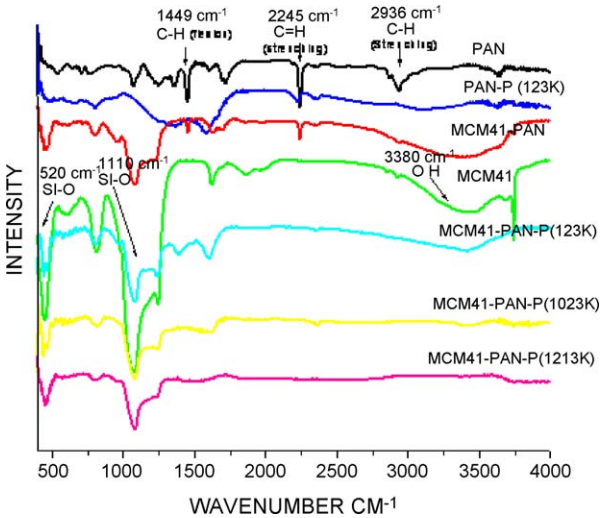

Fig. 7. IR spectra of the series of the initial support MCM-41 and the carbonized supports.

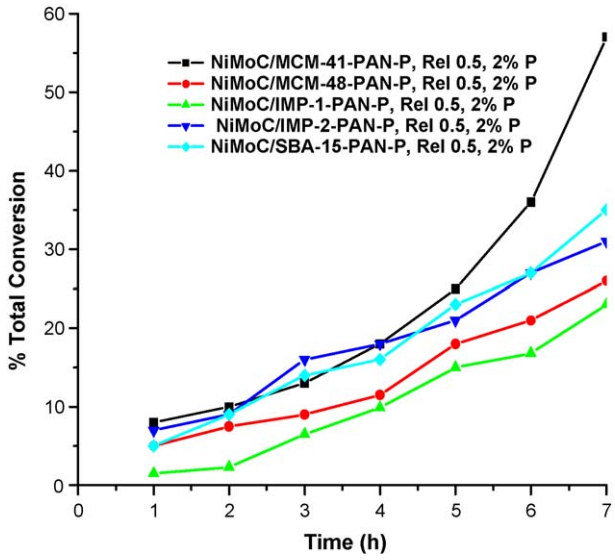

Fig. 8. Catalytic activity of the supported Ni-Mo catalysts at $T = 673$ K and $P = 1$ atm. All the catalysts were carbonized at 1273 K.

redox treatments, *i.e.*, carboxyl, lactone, carbonyl and metoxy type surface groups, but another seat of acidity is due to the surface phosphoric acid type sites, *i.e.*, HPO_4^-, which are formed after impregnation of the solids with ammonium phosphate, which was used as a doping agent and incorporated to the catalysts by the incipient wetness technique

3.4. Catalytic properties

Fig. 8 illustrates the conversion data corresponding to the catalytic activity of the supported bimetallic NiMo carbide catalysts, which were loaded with about 2% Phosphorous and with a metal atomic ratio of 0.5, as described in the experimental section. The initial supports were the MCM-41, MCM-48, IMP-1, IMP-2, and SBA-15. Thus, the overall conversion of n-octane on these catalysts (Fig. 8) indicates that the NiMoC/IMP-1-PAN-P catalyst (metal ratio = 0.5, with 2% P) causes a conversion of about 22.5% after 7 h under stream, while the other catalysts display distinct activity levels at the same period of time, *i.e.*, NiMoC/IMP-1-PAN-P(22.5%) < NiMoC/MCM-48-PAN-P(27%) < NiMoC/IMP-2-PAN-P(30%) < NiMoC/SBA-15-PAN-P(35%) < NiMoC/MCM-41-PAN-P(56%).

Table 5 shows the selectivity data corresponding to four NiMo bimetallic carbide catalysts, where one observes some interesting features about the behavior of each catalyst. For example the

Table 5
Selectivity of the supported NiMoC bimetallic carbide catalysts in function of the time of reaction (h).

Catalysts	Products distribution		
	(%)	t_m: 4 h	t_f: 7 h
NiMoC/MCM-41-PAN-P	n(C_4) 100	n(C_4) 100	n(C_4) 100
NiMoC/MCM-48-PAN-P	n(C_3) 5% n(C_4) 4% n(C_5) 13% n(C_7) 26%	n(C_4) 30% n(C_7) 70%	n(C_4) 13 n(C_4) 2% n(C_5) 15% n(C_7) 70%
NiMoC/IMP-1-PAN-P	n(C_7) 100%	n(C_7) 100%	n(C_7) 100%
NiMoC/IMP-2-PAN-P	n(C_5) 35% n(C_7) 65%	n(C_5) 62% n(C_7) 38%	n(C_5) 92% n(C_7) 8%
NiMoC/SBA-15-PAN-P	n(C_3) 50% n(C_4) 50%	n(C_3) 8% n(C_4) 24% n(C_5) 23% n(C_7) 45%	n(C_3) 12% n(C_4) 10% n(C_5) 34% n(C_7) 44%

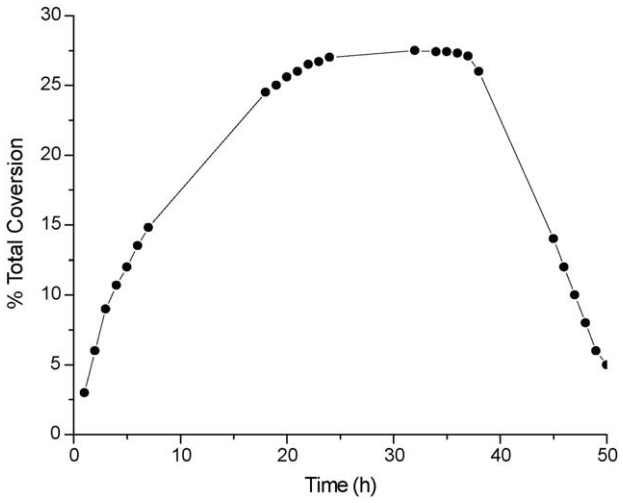

Fig. 9. Catalytic activity of the NiMoC/MCM-41-PAN-P catalysts at $T = 673$ K and $P = 1$ atm.

catalysts NiMoC/MCM-41-PAN-P (metal ratio = 0.5, with 2% P) are selective to the formation of n-butane as the main reaction product almost exclusively, while the NiMoC/MCM-48-PAN-P catalysts (metal ratio = 0.5, with 2% P) are selective to the formation of several products, *i.e.*, n-butane (5%), n-pentane (4%), n-hexane (13%), and n-heptane (26%) during the first reaction hour, while at the fourth hour under stream only n-butane and n-heptane remain. Surprisingly, the NiMoC/IMP-1-PAN-P catalyst (metal ratio = 0.5, with 2% P) is 100% selective to the formation of n-heptane all along the period of reaction, while the NiMoC/IMP-2-PAN catalyst (metal ratio = 0.5, with 2% P) are selective to n-propane (35%) and n-heptane (65%) all along the reaction. Finally, the NiMoC/SBA-15-PAN-P catalysts (metal ratio = 0.5, with 2% P) are selective to n-propane (50%) and n-butane (50%) but n-hexane and n-heptane appear after 4 h of reaction. These results lead us to conclude that the catalysts evolve during the reaction and the active phases undergo through structural changes except for two cases, *i.e.*, NiMoC/MCM-41-PAN-P and NiMoC/IMP-1-PAN-P, where n-C_4 and n-C_7 are promoted with respect to the other products all along the reaction.

The highest conversion of n-octane by hydrocracking over the NiMoC/MCM-41-PAN-P catalysts led to further evaluation for longer reaction periods (50 h) in order to reach the pseudo-stable state. This catalyst presents an extended induction period of about

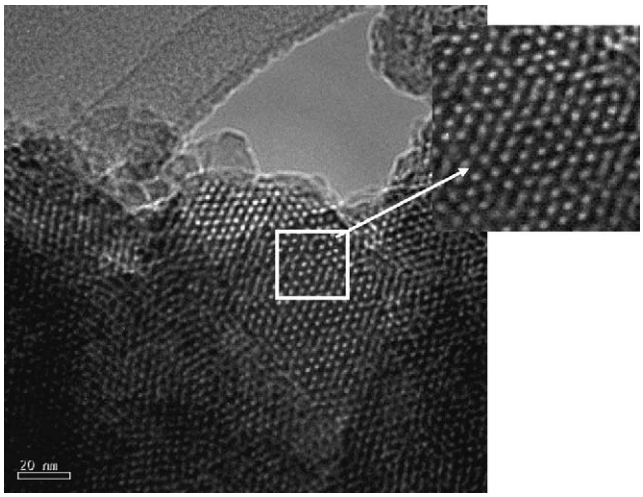

Fig. 10. HRTEM image showing the pore arrays with a hexagonal symmetry of initial MCM-41 support.

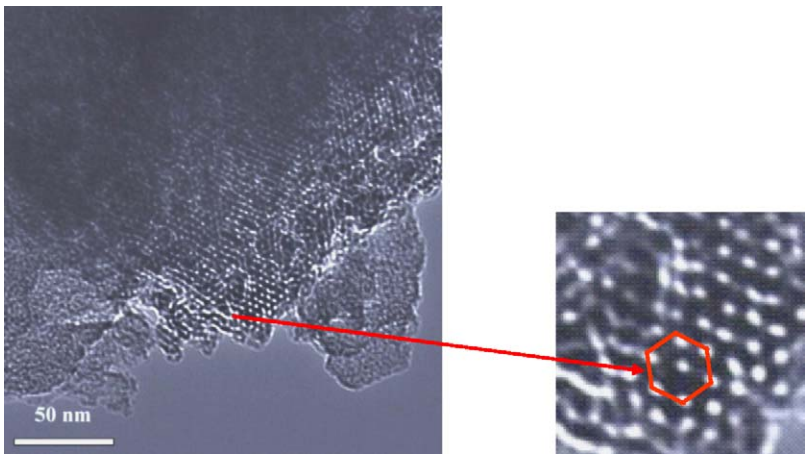

Fig. 11. HRTEM image showing the pore arrays of MCM-41 carbonized at 1273 K. Notice the variations of hexagonal symmetry of the pore arrays.

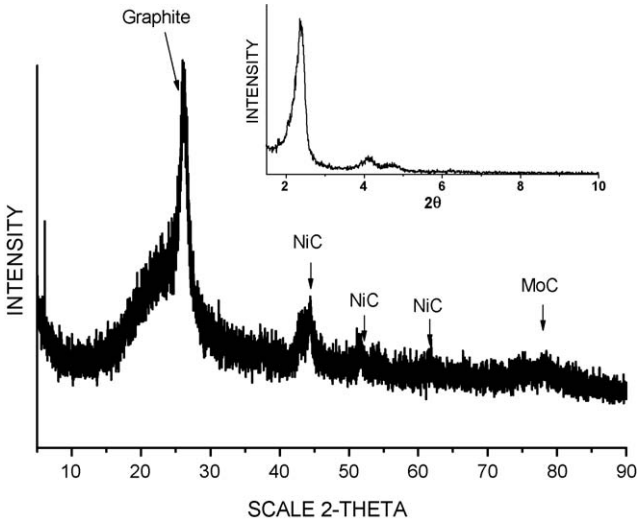

Fig. 12. X-ray diffraction pattern of the NiMoC/MCM-41-PAN-P catalyst after the n-octane hidrocracking reaction. Notice that the characteristic peak of the support is maintained after reaction (inset).

7 h, which coincides with the period of formation of carbon nanofibers that could occur by selective cracking and successive dehydrogenation of n-octane, together with carbon diffusion through the metal particles [14,15], with lower hydrocarbons remaining as products. The formation of carbon nanofibers and their association with metal particles is illustrated in Figs. 14 and 15, where a metal crystallite appears at one end of a hollow carbon nanofiber. Also, a second stability stage (pseudo-stable state) was observed after 18 h under stream and it remains during 40 h, then decreases systematically (deactivation stage) until the reaction ends at about 50 h under stream (Fig. 9).

4. Discussion and conclusions

In general, the surface area of the initial materials was drastically reduced after the series of treatments by monomer (AN) impregnation and subsequent polymerization and carbonization (Tables 1–2). Also, the metal (Ni,Mo) incorporation to the carbonized materials emphasized these effects (Table 2) while the wall thickness increased substantially upon carbonization, *i.e.*, from 1.5 to 2.5 times (Table 1), with respect to the initial materials, which can be attributed to the carbon deposition at the pore mouths and within the pore channel system. Also, symmetry distortions of the pore arrays were verified by TEM (Fig. 11) with respect to the initial material (Fig. 10), as a consequence of the carbonization treatments at 723–1273 K and further reduction under hydrogen and in the presence of hydrocarbons at high temperatures. All these treatments cause a partial collapse of the porous structure but the XRD study shows that the main pore periodicities remain, although in minor proportion, which was verified by the diminution of the XRD intensity peaks and the lower pore size distribution (Figs. 2 and 4). Also, it was shown that the presence of Ni and Mo metals in the carbonized materials promote the graphitization of carbon (Fig. 3) while the MCM-41 characteristic XRD peak loses intensity as a consequence of the partial collapse of the pore system and carbon deposition, but the materials present a sharp XRD peak after the reaction, thus indicating the reinforcement of the pore periodicities (see inset of Fig. 12). In parallel, the TEM results confirm the formation of carbon nanofibers with graphite layers arranged in a herring-bone pattern (Fig. 13B), which explains the appearance of a strong XRD peak at about 25° (2θ), as shown in Fig. 3. Those fibers are more probably produced by an extrusion-like process by diffusion of carbon atoms through the metal particles [15]. In a methane reductive atmosphere the nickel carbide phases favor the growth of carbon nanofibers, specifically on the exposed planes such as (1 1 0), (1 0 0), and (1 1 1), while the carbon nanofibers are about 0.1 μm wide with approximately 5 μm length, with graphitic planes around the fiber walls (Fig. 13A and B). Also, the TEM bright field image of a single carbon nanofiber with a metal particle inside (Fig. 14A) shows clearly the inner hollowness left by the particle along the fiber, while Fig. 14B shows the same fiber observed by HAAD (High Angle Annular Detector), a technique that is very sensitive to atomic number (*Z*-contrast), where one observes clearly the metal particle of about 25 nm diameter and the outline of the carbon fiber in the background. In addition, the HAAD image of Fig. 15 corresponds to the region (at left) shown in Fig. 14 and its X-ray map corresponding to Carbon (upper right-hand side), Nickel (lower left-hand side) and Molybdenum (lower right-hand side). In this series one observes the silhouette of the carbon fiber on the upper right-hand side of Fig. 15, which indicates the carbon X-ray emission from the fiber, which includes the contour of the carbon fiber surrounding the metal particle, thus indicating either a confinement of the particle by the carbon fiber or a metal particle that is composed of two elements, Ni and C. *i.e.* Nickel carbide. In addition, the X-ray map of the metal particle in the lower left-hand side indicates the typical energy emission from Nickel, which is more intense than the X-ray signal arising from Molybdenum (*i.e.*, lower right-hand side). Other regions show about similar features, but the Molybdenum X-ray emission seems dim and more scattered than Nickel along the fibers.

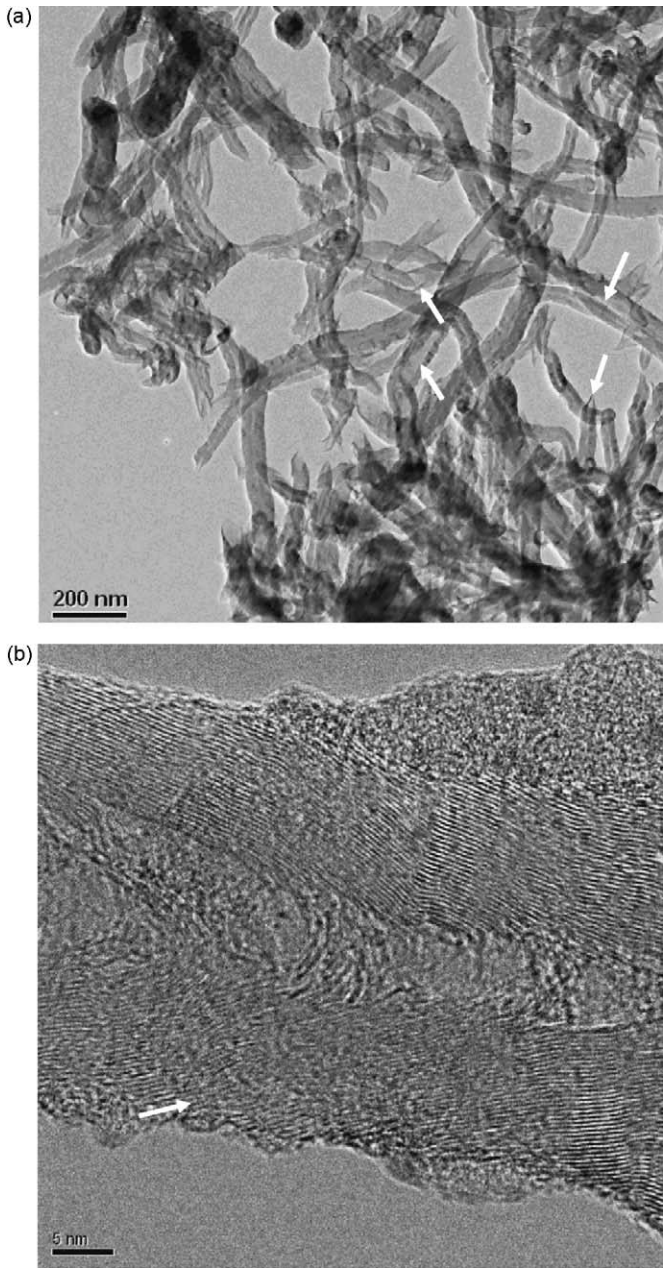

Fig. 13. (A) TEM micrograph corresponding to NiMoC/MCM-41-PAN materials. Notice the hollow carbon nanofibers (arrowed). (B) High resolution TEM micrograph of a single fiber showing the graphitic planes.

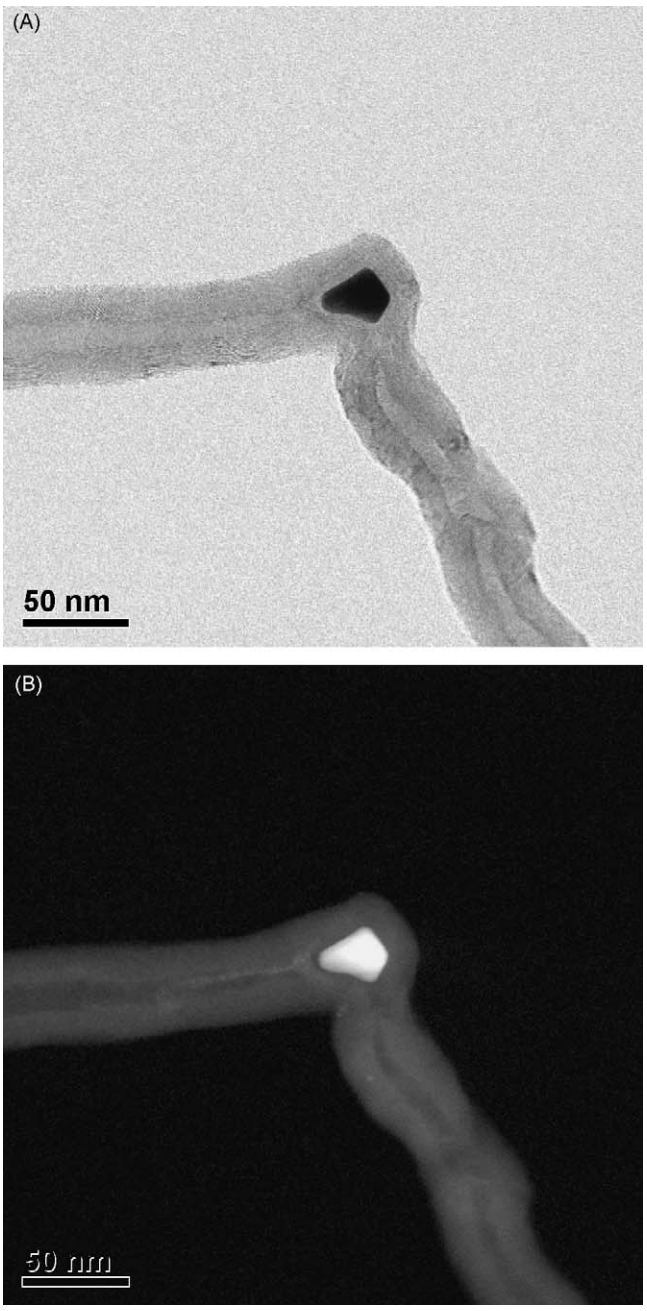

Fig. 14. (A) Bright field image showing a carbon nanofiber with a metal particle inside, (B) HAAD image of the same region (HAAD is sensitive to atomic number, *i.e.*, *Z*-contrast).

On the other hand, the materials having the highest surface acidity are those showing the highest conversion of n-octane. In general, the NiMo supported catalyst series with mesoporous supports such as MCM-41, MM-48, IMP-1, IMP-2, and SBA-15 showed distinct levels of activity, but the highest conversion of n-octane was obtained with the NiMoC/MCM-41-PAN-P catalyst (metal ratio = 0.5, 2% P), with a marked selectivity to n-butane. In general, the NiMo carbide catalysts supported on the MCM-41 mesoporous materials presented a high conversion after the 7 h period of induction, from 56 to 90%, with high selectivity towards the formation of pure n-paraffins, in particular the NiMoC/MCM-41-PAN-P and NiMoC/IMP-1-PAN-P catalysts with a metal ratio of 0.5 (with 2% P) are 100% selective to the formation of n-butane and n-heptane, respectively. Although this mechanism is not fully understood, it seems as if n-octane is broken down in a specific carbon in the chain, *i.e.*, the alpha carbon in the case of the IMP-1-P supported catalyst, then the carbon atom diffuses through the metal particle and it starts forming a carbon nanofiber, while the hydrocarbon fraction left (*i.e.*, n-heptane) remains. Thus, the n-octane conversion is split between the selective hydrocracking (alpha carbon) to lower hydrocarbons [16] and the formation of carbon fibers. There are hydrocarbon products left after the injection of carbon ti the metal particles, which are in the range from propane to n-heptane, while methane and ethane were rarely detected in this reaction. This is interpreted as the period needed for a successive series of reactions comprising dehydrogenation, cracking and carbon atoms diffusion through the metal particles, with a re-hydrogenation of unsaturated compounds afterward, thus producing carbon nanofibers and lower hydrocarbons at the end. This series of reactions might stop after the encapsulation of

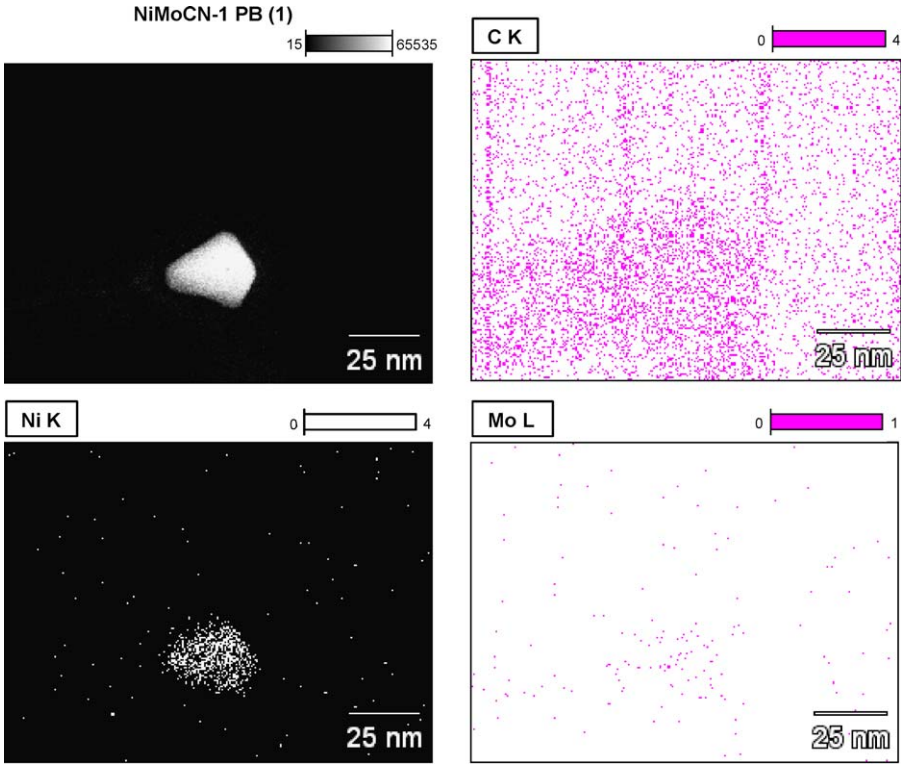

Fig. 15. HAAD image (upper left side) and the X-ray mappings (right) corresponding to carbon (upper right side) nickel (lower left side) and molybdenum (lower right side).

the metal particles but the activity still remains due to the smaller metal clusters spreaded on along the carbon fibers. The TEM results indicate that nickel is more frequently in the form of metal particles but molybdenum is rather scattered along the carbon fibers. Also, XRD results indicate that in both cases the metal carbides are apparent and exist in separated phases, which lead us to conclude that each phase contributes to the catalytic conversion of the n-paraffins in a separated pathway. Most of the Nickel particles were found encapsulated by the carbon left after the reaction, which means that this metal could act as a catalyst more probably at the initial stages of the reaction but later the Mo clusters could take the lead until complete carbon coverage.

Acknowledgments

The authors acknowledge the IMP and CONACYT for financial support, and especially Victor M. Menendez for his support in X-ray diffraction studies.

References

[1] (a) Xiaohui Zhang, Martin Chodakowski, John M. Shaw, Energy Fuels 19 (4) (2005) 1405–1411;
(b) V. Rabarihoela-Rakotovao, F. Diehl, S. Brunet, Catal. Lett. 129 (2009) 50–60;
(c) J.G. Speight, The Desulfurization of Heavy Oils and Residua, Marcel Dekker Inc., New York, 2000, p. 193;
(d) P. Rahimi, T. Gentzis, E. Cotté, Energy Fuels 13 (1999) 694.
[2] (a) M.J. Girgis, Y.P. Tsao, Impact of catalyst metal–acid balance in n-hexadecane hydroisomerization and hydrocracking, Ind. Eng. Chem. Res. 35 (1996) 386–396;
(b) H. Ling, Q. Wang, Ben-xian Shen, Hydroisomerization and hydrocracking of hydrocracker bottom for producing lube base oil, Fuel Processing Technol. 90 (2009) 531–535;
(c) Hiromichi Shimada, Koichi Sato, Kosaku Honna, Toshiyuki Enomoto, Nobuyasu Ohshio, Catal. Today 141 (2009) 43–51;
(d) A. Corma, A. Martínez, J. Catal. 25–31 (1995) 153.
[3] M.J. Ledoux, C. Pham, J. Guille, H. Dunlop, J. Catal. 383 (1992) 134.
[4] N. Tsubaki, J. Chang, Y. Yoneyama, K. Fujimoto, J. Jpn. Petrol Inst. 45 (2) (2002) 77.
[5] S.K. Saha, G.K. Biswas, D. Biswas, Stud. Surf. Sci. Catal. 142A (2002) 771.
[6] J.S. Beck, J.C. Vartulli, J. Am. Chem. Soc. 2317–2326 (1992) 114.
[7] M. Kruk, M. Jaroniec, S. Hoon Joo, R. Ryoo, J. Phys. Chem. B 107 (2003) 2205–2213.
[8] (a) D. Zhao, J. Feng, Q. Huo, N. Melosh, G.H. Fredrickson, B.F. Chmelka, G.D. Stucky, Science 279 (1998) 548;
(b) D. Zhao, Q. Huo, J. Feng, B.F. Chmelka, G.D. Stucky, J. Am. Chem. Soc. 120 (1998) 6024;
(c) C. Goltner-Spickermann, Curr. Opin. Interface Colloid Sci. 7 (2002) 173;
(d) C.-F. Cheng, Y.-C. Lin, H.-H. Cheng, Y.-C. Chen, Chem. Phys. Lett. 382 (2003) 496.
[9] (a) J.M. Domínguez-Esquivel, E. Terres-Rojas, A. Vázquez, Microporous Mesoporous Mater. 341–348 (2003) 66;
(b) M. Dominguez José, Rosas Raúl, Aburto Jorge, Terrés Eduardo, López Alfonso, Martínez-Palou Rafael, Synthesis of silica spheres with neutral and ionic amphiphiles and their interaction with photosensitive spiropyrans, Microporous Mesoporous Mater. 118 (2009) 121–133.
[10] L. Volpe, M. Boudart, Compounds of molybdenum and tungsten with high specific surface area. II. Carbides, J. Solid State Chem. 332–347 (1985) 59.
[11] V.B. Fenelonov, V. Romannikov, N. Derevyankin, A. Yu, Microporous Mesoporous Mater. 28 (1999) 57.
[12] A.I. Reyes de la Torre, J.A. Melo-Banda, R. Garcia-Alamilla, G. Sandoval-Robles, E. Terres-Rojas, A. Lopez-Ortega, J.M. Dominguez, J. Phys.: Condens. Matter. 16 (2004) S2329–S2334.
[13] Philippe Serp, Massimiliano Corrias, Philippe Kalck, Carbon nanotubes nanofibers in catalysis, Appl. Catal. A: Gen. 253 (2003) 337–358.
[14] M. Audier, A. Oberlin, M. Coulon, Crystallographic orientations of catalytic particles in filamentous carbon; Case of simple conical particles, J. Crys. Growth 55 (December (3)) (1981) 549–556.
[15] F.C. Schouten, O.L.J. Gijzeman, G.A. Bootsma, Stud. Surf. Sci. 87 (1979) 460.
[16] M. Guisnet, C. Thomazeau, J. Catal. 102–110 (1995) 152.